processes

MDPI

*Article*

# Transformer Core Loosening Diagnosis Based on Fusion Feature Extraction and CPO-Optimized CatBoost

**Yuanqi Xiao, Yipeng Yin, Jiaqi Xu and Yuxin Zhang ***

The College of Electrical and Information Engineering, Beihua University, Jilin 132021, China; yq.xiao.bhu@outlook.com (Y.X.); yinyipeng202509@163.com (Y.Y.); xujiaqi202509@163.com (J.X.)
* Correspondence: zhangyuxinbh@beihua.edu.cn

**Abstract**

Transformer reliability is crucial to grid security, with core loosening a common fault. This paper proposes a transformer core loosening fault diagnosis method based on a fusion feature extraction approach and Categorical Boosting (CatBoost) optimized by the Crested Porcupine Optimizer (CPO) algorithm. Firstly, the audio signal is decomposed into six Intrinsic Mode Functions (IMF) components through Variational Mode Decomposition (VMD). This paper utilizes Gaussian membership functions to quantify the energy proportion, central frequency, and kurtosis of IMF and constructs a fuzzy entropy discrimination function. Then, the IMF noise components are removed through an adaptive threshold. Subsequently, the denoised signal undergoes a wavelet packet transform instead of a short-time Fourier transform to optimize Mel-frequency cepstral coefficients (WPT-MFCC), combining time-domain statistical features and frequency-band energy distribution to form a 24-dimensional fusion feature. Finally, the CatBoost algorithm is employed to validate the effects of different feature schemes. The CPO is introduced to optimize its iteration number, learning rate, tree depth, and random strength parameters, thereby enhancing overall performance. The CPO-optimized CatBoost model had 99.0196% fault recognition accuracy in experimental testing, 15% better than the standard CatBoost. Accuracy exceeded 90% even under extreme 0 dB noise. This method makes fault diagnosis more accurate and reliable.

**Keywords:** transformer core loosening; VMD; WPT-MFCC; CPO; CatBoost

check for updates

Academic Editor: Maoyin Chen

Received: 16 September 2025
Revised: 10 October 2025
Accepted: 10 October 2025
Published: 12 October 2025

**Citation:** Xiao, Y.; Yin, Y.; Xu, J.; Zhang, Y. Transformer Core Loosening Diagnosis Based on Fusion Feature Extraction and CPO-Optimized CatBoost. *Processes* **2025**, *13*, 3247. https://doi.org/10.3390/pr13103247

**Copyright:** © 2025 by the authors. Licensee MDPI, Basel, Switzerland. This article is an open access article distributed under the terms and conditions of the Creative Commons Attribution (CC BY) license (https://creativecommons.org/licenses/by/4.0/).

## 1. Introduction

As a core device in the power system, the operational reliability of power transformers is directly related to the safety of the power grid. Core loosening is a common mechanical fault in transformers, which is caused by factors such as electromagnetic vibration, thermal stress, and material aging [1]. This fault can lead to increased vibration and noise and, in severe cases, cause equipment damage [2]. Traditional offline detection requires power outages for maintenance, affecting the continuity of the power supply [3]. Acoustic signal recognition technology enables non-contact online diagnosis by analyzing the operational sound signals, featuring strong real-time performance and low cost. The online monitoring technology based on acoustic signal analysis has become a research hotspot due to its non-intrusive and real-time advantages [4]. It is of great significance for improving the intelligent operation and maintenance level of transformers.

In the field of equipment fault diagnosis, signal decomposition and feature optimization serve as the core aspects for enhancing diagnostic accuracy. Variational mode decomposition (VMD) can adaptively decompose signals into band-limited intrinsic mode

functions (IMF) [5]. However, it has not been optimized for the specific scenarios of fault diagnosis and lacks the ability to actively screen for fault-related modes. Liu et al. [6] used the central frequency of VMD to focus on fault frequencies but did not solve the problem of frequency interval confusion caused by noise, making it difficult to accurately distinguish between normal and fault frequencies. Xue Jiantong et al. [7] constructed transformer fault feature vectors through VMD energy entropy, but only energy entropy has insufficient discrimination ability under complex noise and is prone to misjudging low-energy fault modes. Jiao et al. [8] combined VMD with kurtosis to enhance the ability to capture impulse signals. However, the sensitivity of kurtosis to multi-impulse superposed signals decreases, rendering this method unable to comprehensively reflect fault characteristics. Therefore, to address these problems where a single indicator shows poor performance, after VMD decomposition, Gaussian membership functions are constructed based on the energy proportion, central frequency, and kurtosis. Then, by calculating the adaptive threshold of fuzzy entropy, precise screening of noise modes can be achieved.

The quality of feature extraction directly determines the diagnostic effectiveness. The Mel-Frequency Cepstral Coefficients (MFCC) can effectively represent the spectral envelope. Therefore, MFCC is widely applied in both speech signal recognition [9–12] and fault diagnosis [13–17]. They can capture the subtle spectral changes of faults. Wang Fenghua et al. applied MFCC to the acoustic signal recognition of transformers [18], confirming its value in extracting the fault features of transformers. However, this study did not address the limitations of traditional MFCC technology. Traditional MFCC relies on the Short-Time Fourier Transform (STFT), which has the drawback of being unable to balance time and frequency resolutions simultaneously [19]. In contrast, the Wavelet Packet Transform (WPT) can adaptively divide frequency bands and accurately extract the fault features in different frequency intervals [20]. For this reason, this paper proposes a 24-dimensional WPT-MFCC fusion feature, integrating the advantages of both to enhance the discrimination of fault features.

The performance of classification models is crucial for the reliability of diagnosis. As a Gradient Boosting Decision Tree algorithm, Categorical Boosting (CatBoost) has demonstrated excellent classification accuracy in bearing fault diagnosis [21] and can be extended to the field of power transformer fault identification [22], effectively handling high-dimensional features and class imbalance issues. However, the performance of CatBoost is highly dependent on the setting of hyperparameters. Traditional grid search is inefficient, while new meta-heuristic algorithms offer new approaches for parameter optimization [23–25]. The Crested Porcupine Optimizer (CPO) algorithm, by simulating the defense mechanism of the porcupine, achieves a good balance between global search and local exploitation [26]. Therefore, this paper adopts CPO to optimize the key parameters of CatBoost, further enhancing the diagnostic accuracy and stability.

In summary, this paper proposes a transformer core looseness fault diagnosis method based on VMD, 24-dimensional fusion feature extraction of WPT-MFCC, and CPO-CatBoost. VMD is used to decompose the collected acoustic signal in the experiment to obtain IMF components, and the noise components are identified by calculating their fuzziness and combining with adaptive thresholds. Then, the improved 24-dimensional MFCC is used to extract data from the signal. During the training of the CatBoost model, CPO is used to optimize its iteration number, learning rate, tree depth, and random strength parameters, and the CPO-CatBoost model is constructed to identify and diagnose the transformer core looseness fault.

## 2. Materials and Methods

### *2.1. VMD Decomposition Operation*

The Variational Mode Decomposition (VMD) algorithm was proposed by Dragomiretskiy et al. [27] in 2014. Different from signal decomposition methods such as Empirical Mode Decomposition (EMD), VMD is an iterative rather than recursive adaptive signal decomposition algorithm [28]. It decomposes the original signal into k Intrinsic Mode Functions (IMF) with specific central frequencies by solving variational problems.

$$\min_{\{u_k\},\{\omega_k\}} \left\{ \sum_{k=1}^{K} \left\| \partial_t \left[ \left( \delta(t) + \frac{j}{\pi t} \right) * u_k(t) \right] e^{j\omega_k t} \right\|_2^2 \right\}, \quad \text{s.t.} \sum_{k=1}^{K} u_k(t) = f(t) \tag{1}$$

where $u_k(t)$ denotes the k-th modal component; $\omega_k$ denotes the central frequency of the k-th mode; $\delta(t)$ represents the Dirac delta function; $*$ denotes convolution and $j$ is the imaginary unit; $\partial_t \left[ \left( \delta(t) + \frac{j}{\pi t} \right) * u_k(t) \right]$ denotes the derivative of the Hilbert transform of $u_k(t)$; the norm $\| \|_2^2$ represents energy, with the overall objective being to minimise the "frequency bandwidth" of each mode.

The constrained problem is addressed by incorporating the augmented Lagrangian function into the objective function.

$$L(\{u_k\},\{\omega_k\},\lambda) = \alpha \sum_{k=1}^{K} \left\| \partial_t \left[ \left( \delta(t) + \frac{j}{\pi t} \right) * u_k(t) \right] e^{-j\omega_k t} \right\|_2^2 + \left\| f(t) - \sum_{k=1}^{K} u_k(t) \right\|_2^2 + \left\langle \lambda(t), f(t) - \sum_{k=1}^{K} u_k(t) \right\rangle, \tag{2}$$

where $\alpha$ is the penalty parameter, controlling the weight of the reconstruction errors; $\lambda(t)$ is the Lagrange multiplier, used to constrain to ensure that "the sum of the modes equals the original signal"; $\langle , \rangle$ denotes the inner product.

The above variational problem is solved by iteratively updating $u_k(t)$, $\omega_k$, and $\lambda$.

Update of IMF:

$$\hat{u}_k^{n+1}(\omega) = \frac{\hat{f}(\omega) - \sum_{i \neq k} \hat{u}_i(\omega) + \frac{\hat{\lambda}(\omega)}{2}}{1 + 2\alpha(\omega - \omega_k)^2}, \tag{3}$$

where $\hat{f}(\omega)$ denotes the Fourier transform of the original signal; $\sum_{i \neq k} \hat{u}_i(\omega)$ represents the sum of the frequency domain components of other modes; $\hat{\lambda}(\omega)$ denotes the frequency domain representation of the Lagrange multiplier.

Update of the central frequency:

$$\omega_k^{n+1} = \frac{\int_0^\infty \omega |\hat{u}_k(\omega)|^2 d\omega}{\int_0^\infty |\hat{u}_k(\omega)|^2 d\omega}, \tag{4}$$

Update of the Lagrange multiplier:

$$\hat{\lambda}^{n+1}(\omega) = \hat{\lambda}^n(\omega) + \tau \left( \hat{f}(\omega) - \sum_{k=1}^{K} \hat{u}_k^{n+1}(\omega) \right), \tag{5}$$

where $\tau$ denotes the update step size.

Stop when the difference between the modal components of adjacent iterations is less than the threshold tol:

$$\sum_{k=1}^{K} \left\| \hat{u}_{k,+}^{(n)} - \hat{u}_{k,+}^{(n-1)} \right\|_2^2 < \text{tol}, \tag{6}$$

*2.2. Fuzzy Entropy Construction*

After conducting VMD decomposition on the acoustic fingerprint signals of transformer core looseness to obtain K layers of IMFs, the information in three dimensions, namely the energy proportion, central frequency, and kurtosis, is integrated. By introducing the Gaussian membership function, fuzzy entropy is constructed. This fuzzy entropy serves as an index to quantify the degree of uncertainty regarding whether a signal component belongs to noise. Through the use of an adaptive threshold, soft decision-making between noise and signal components is realized. This approach effectively avoids the misjudgment of boundary IMFs and enhances the recognition of noise components.

Three features are calculated for the decomposed IMF components $u_k(t)$:

(1) Energy proportion (the contribution of the IMF component to the total signal):

$$E_k = \frac{\sum_{n=1}^{N} u_k^2(n)}{\sum_{i=1}^{K} \sum_{n=1}^{N} u_i^2(n)} \times 100\%, \tag{7}$$

where $\sum_{n=1}^{N} u_k^2(n)$ denotes the total energy of the k-th IMF; $\sum_{i=1}^{K} \sum_{n=1}^{N} u_i^2(n)$ denotes the sum of the total energies of all IMF components.

(2) The formula for the normalized central frequency (frequency domain distribution characteristics of IMF):

$$f_{c,k} = \frac{\sum_m f_m \cdot |U_k(f_m)|}{\sum_m |U_k(f_m)|} \quad \bar{f}_{c,k} = \frac{f_{c,k}}{f_s/2}, \tag{8}$$

where $f_m$ represents the frequency value at the m-th frequency point, $U_k(f_m)$ is the complex spectral value of the k-th IMF at the frequency $f_m$, and $f_s/2$ is the Nyquist frequency.

(3) Kurtosis serves to characterize the peakiness of a signal. In scenarios involving impulsive components, such as the case of a loose transformer core, the noise generally exhibits a relatively high kurtosis value. The formula for kurtosis is as follows:

$$\mathrm{Kurt}_k = \frac{E\left[(u_k - \mu_k)^4\right]}{\sigma_k^4}, \tag{9}$$

where $\mu_k$ denotes the mean of the k-th IMF, $\mu_k = \frac{1}{N}\sum_{n=1}^{N} u_k(n)$; $\sigma_k$ denotes the standard deviation of the k-th IMF, $\sigma_k = \sqrt{\frac{1}{N}\sum_{n=1}^{N} (u_k(n)-\mu_k)^2}$; and $E[\,]$ represents the expectation operator.

Calculate the membership degrees of each feature with respect to noise and signal using the Gaussian membership function:

$$\mu(x; c, \sigma) = \exp\left(-\frac{(x-c)^2}{2\sigma^2}\right), \tag{10}$$

Comprehensive membership degree:

$$\mu_{\text{noise}} = \frac{\mu_{\text{noise energy}} \cdot \mu_{\text{noise, freq}} \cdot \mu_{\text{noise, kurt}}}{\mu_{\text{noise, total}} + \mu_{\text{signal, total}} + \epsilon} \quad \mu_{\text{signal}} = \frac{\mu_{\text{signal, energy}} \cdot \mu_{\text{signal, freq}} \cdot \mu_{\text{signal, kurt}}}{\mu_{\text{noise, total}} + \mu_{\text{signal, total}} + \epsilon}, \tag{11}$$

Specifically, $\mu_{\text{noise}}$ and $\mu_{\text{signal}}$ represent the comprehensive membership degrees of noise and signal, respectively. $\mu_{\text{noise energy}}$, $\mu_{\text{noise, freq}}$, and $\mu_{\text{noise, kurt}}$ denote the membership degrees of noise regarding the energy proportion, central frequency, and kurtosis. These values fall within the range of $[0, 1]$. Similarly, $\mu_{\text{signal, energy}}$, $\mu_{\text{signal, freq}}$, and $\mu_{\text{signal, kurt}}$ are the membership degrees of the signal, corresponding to the same parameters as those of noise. $\mu_{\text{noise, total}}$ and $\mu_{\text{signal, total}}$ are the products of the membership degrees of each feature of noise and signal, respectively.

Basic entropy (Shannon entropy):

$$H_{base} = -\mu_{noise} \log(\mu_{noise} + \epsilon) - \mu_{signal} \log\left(\mu_{signal} + \epsilon\right), \quad (12)$$

Feature dispersion (standard deviation of the feature vector):

$$\sigma_{feat} = \text{std}([r_k, f_{n,k}, \kappa_k/10]), \quad (13)$$

Final fuzzy entropy:

$$H_k = (H_{base} + \mu_{noise} \cdot 2 + \sigma_{feat}) \cdot \left(1 + \frac{\mu_{noise,energy} + \mu_{naise,freq} + \mu_{noise,kurt}}{3}\right), \quad (14)$$

Adaptive threshold noise detection employs the sum of the mean and standard deviation of all IMF fuzzy entropies as the threshold. The threshold calculation is as follows:

$$\text{threshold} = \mu_H + \sigma_H, \quad (15)$$

where $\mu_H = \frac{1}{K}\sum_{k=1}^{K} H_k$ and $\sigma_H = \text{std}(H_1, \ldots, H_K)$.

Noise Judgment Criterion: If the fuzzy entropy $H_k$ of an IMF satisfies $H_k >$ threshold, then this IMF is identified as a noise IMF.

### *2.3. WPT-MFCC Feature Extraction Algorithm*

The Mel-Frequency Cepstral Coefficients (MFCC) are parameters that can comprehensively reflect the perception characteristics of the human ear [29]. These cepstral coefficients can be extracted from the Mel-scale frequency domain, with the conversion formula between Mel frequencies and linear frequencies given by Equation (16). Owing to their superior noise resistance and robustness, MFCCs represent the most commonly employed features in the field of speech recognition.

$$f_{Mel} = 2595 \lg\left(1 + \frac{f}{700}\right), \quad (16)$$

where $f_{Mel}$ denotes the Mel frequency based on auditory perception, represents the actual linear frequency, measured in hertz (Hz).

The traditional MFCC features are obtained as follows. First, pre-emphasis, framing, and windowing are applied to the signal, and then the Short-Time Fourier Transform (STFT) is carried out to obtain the linear spectrum. Subsequently, a Mel filter bank is utilized to perform weighted summation on the linear spectrum, resulting in the Mel-band energy. Logarithmic compression is then applied to the Mel-band energy. Afterward, the first 13 coefficients are extracted via the Discrete Cosine Transform (DCT) to generate the basic MFCC. Finally, the first-order and second-order differences are computed and combined with the basic MFCC to form a 39-dimensional traditional MFCC feature vector.

Nevertheless, in the context of diagnosing transformer core loosening faults, audio signals typically exhibit non-stationary characteristics [30]. These signals often contain transient impacts and sudden frequency changes. The Short-Time Fourier Transform (STFT) employs a fixed-window approach, which inherently fails to concurrently achieve high-quality time and frequency resolutions. In contrast, the multi-resolution analysis of the Wavelet Packet Transform (WPT) enables the capture of transients using small windows (affording high time resolution) in the high-frequency band and the acquisition of detailed information with large windows (providing high frequency resolution) in the low-frequency band. Furthermore, it can accurately match the frequency band characteristics, non-stationarity, and resolution requirements of the collected signals.

The feature extraction procedure for transformer core loosening signals based on WPT-MFCC is illustrated in Figure 1. Initially, signal pre-processing is conducted. Subsequently, the wavelet packet transform is exploited to decompose the signal frequency band with high precision. Thereafter, within each sub-band, Mel filtering, logarithmic compression, and DCT are executed in succession. Eventually, 24 feature dimensions are extracted. This enables the yield of results that describe the signal's time-frequency characteristics with greater precision.

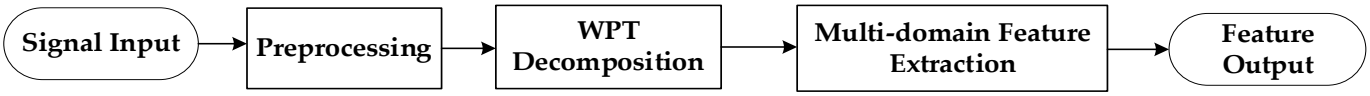



**Figure 1.** WPT-MFCC Feature Extraction Block Diagram.

Following the replacement of STFT with WPT [31–33], dimensional fusion enhancements were applied to the extracted MFCC data, resulting in 24-dimensional MFCCs. WPT:

$$W_j^n(k) = \sum_m h(m - 2k)W_{j-1}^{2n}(m) + \sum_m g(m - 2k)W_{j-1}^{2n-1}(m), \quad (17)$$

where j denotes the number of decomposition levels (four levels are employed in the code) and n represents the node index, while h and g denote the low-pass and high-pass filters respectively (using a db4 wavelet).

Frequency band energy calculation:

$$E_i = \sum_{k=1}^{N_i} |c_i(k)|^2, \quad (18)$$

where $c_i(k)$ is the coefficient at the *i*-th wavelet packet node.

By replacing STFT with WPT for signal processing, the DCT transform is applied to the resulting features. The first eight coefficients are extracted and serve as the first eight dimensions ($F_1$–$F_8$) of the WPT-MFCC feature vector. Dimensions 9–11 ($F_9$–$F_{11}$) represent 10% of the first, fourth, and seventh coefficients of WPT-MFCC; Dimensions 12 and 13 ($F_{12}$ and $F_{13}$) constitute 5% and 10% of the mean of WPT-MFCC; Dimension 14 ($F_{14}$) corresponds to 1% of the absolute sum.

The dimensions from 15 to 19 are the mean $F_{15} = \mu = \frac{1}{N}\sum_{i=1}^{N}$, the standard deviation $F_{16} = \sigma = \sqrt{\frac{1}{N}\sum_{i=1}^{N}(x_i - \mu)^2}$, the kurtosis $F_{17} = K = \frac{1}{N}\sum_{i=1}^{N}\left(\frac{x_i - \mu}{\sigma}\right)^4$, the average absolute value of the signal $F_{18} = MAV = \frac{1}{N}\sum_{i=1}^{N}|x_i|$, and the energy $F_{19} = E = \sum_{i=1}^{N} x_i^2$ in sequence.

For dimensions 20–24, the design of band-pass filters for composite frequency-band energy characteristics is adopted:

$$H(s) = \frac{1}{1 + \left(\frac{s}{\omega_c}\right)^{2n}}, \quad (19)$$

For dimensions 20–22: The 20th dimension represents the low-frequency energy, denoted as $F_{20} = E_{low} = \sum_t |x_{filtered,low}(t)|^2$; the 21st dimension represents the mid-frequency energy, denoted as $F_{21} = E_{mid} = \sum_t |x_{filtered,\,mid}(t)|^2$; and the 22nd dimension represents the high-frequency energy, denoted as $F_{22} = E_{high} = \sum_t \left|x_{filtered,high}(t)\right|^2$.

The 23rd dimension is the spectral centroid:

$$F_{23} = f_c = \frac{\sum_k f_k \cdot |X(k)|}{\sum_k |X(k)|}, \quad (20)$$

where $X(k)$ is the FFT, and $f_k$ is the corresponding frequency.

The 24th dimension corresponds to the zero-crossing rate.

$$F_{24} = ZCR = \frac{1}{N-1}\sum_{i=1}^{N-1} 1[\text{sign}(x_i) \neq \text{sign}(x_{i+1})], \tag{21}$$

where $1[\,]$ is the indicator function.

The newly formed dimensions represent not merely a simple dimensional adjustment of traditional MFCCs, but rather a multi-domain fusion of "time-frequency features, dynamic differences, global statistics, and frequency-domain segmentation", ultimately yielding a 24-dimensional WPT-MFCC. This approach retains the spectral perception characteristics of conventional MFCCs while enhancing the description capability for non-stationary signals through wavelet packet transform and multi-domain features, making it suitable for feature extraction from complex audio signals.

### *2.4. CPO-CatBoost Fault Diagnosis Model*

#### 2.4.1. CatBoost Model

Categorical Boosting (CatBoost) is an ensemble learning algorithm based on Gradient Boosted Decision Trees (GBDT) [34,35], specifically designed to handle categorical features and mitigate overfitting. Its core strengths lie in its Ordered Boosting strategy and efficient handling of categorical features.

The model iteratively constructs multiple decision trees. Each tree is trained based on the prediction error (gradient) of the previous tree. The final output is the weighted sum of all the trees. For an input feature vector x, the classification prediction formula is:

$$\hat{y}(x) = \hat{y}_0 + \sum_{m=1}^{M} \eta \cdot f_m(x, D, \gamma), \tag{22}$$

where M denotes the iteration number, $\eta$ represents the learning rate, D signifies the tree depth, and $\gamma$ indicates the random strength.

#### 2.4.2. CPO Optimization Algorithm

CPO (Crested Porcupine Optimizer) is a meta-heuristic optimisation algorithm simulating the defensive behaviour of the crested porcupine. Proposed by Abdel-Basset in 2024 [36], it locates optimal solutions through two phases [37]: exploration (expanding the search scope) and exploitation (refining local search). This approach is well-suited for optimisation problems involving complex parameter spaces.

The probability that a crested porcupine uses the exploration and exploitation phases each time is equivalent. Moreover, each phase has two different mechanisms. During the exploration phase, the search scope is expanded through global search to cover more areas of the solution space, thereby preventing the algorithm from getting trapped in local optima. For the first defense mechanism, which mimics the "individual vigilant wandering" of crested porcupines, the intermediate position is calculated as follows:

$$y_t = \frac{X_i + X_{rand}}{2}, \tag{23}$$

Position update:

$$X_i^{new} = X_i + randn \times \left| 2 \times rand \times X_{best} - y_t \right|, \tag{24}$$

where $X_{rand}$ denotes the randomly selected individual position, and $X_{best}$ represents the current optimal solution.

The second defensive mechanism emulates the "collective collaborative exploration" behavior of crested porcupines:

$$X_i^{new} = U_1 \times X_i + (1 - U_1) \times (y_t + \text{rand} \times (X_{r2} - X_{r3})), \tag{25}$$

where $U_1$ is a binary vector (whose elements are randomly 0 or 1), and $X_{r2}$ and $X_{r3}$ are randomly selected individual positions.

The core objective of the exploitation phase is to conduct a refined search. It involves in-depth optimization within the high-quality regions identified during the exploration phase to enhance the accuracy of the solution.

The third defense mechanism, which emulates the "focused excavation" of crested porcupines, entails the calculation of fitness-related parameters:

$$S_t = \exp\left(-\frac{f_i}{\sum|f_i| + \epsilon}\right), \tag{26}$$

$$Y_t = 2 \times \text{rand} \times \left(1 - \frac{t}{T_{max}}\right)^{\frac{t}{T_{max}}}, \tag{27}$$

Position update:

$$X_i^{new} = (1 - U_1) \times X_i + U_1 \times (X_{r1} + S_t \times (X_{r2} - X_{r3}) - S), \tag{28}$$

where $S = \text{rand} \times U_2 \times Y_t \times S_t$, $U_2$ is a random vector taking values of $-1$ or 1.

The fourth defense mechanism, which emulates the "intensive exploration around the optimal solution" of crested porcupines, involves calculating the movement factor:

$$M_t = \exp\left(-\frac{f_i}{\sum|f_i| + \epsilon}\right), \tag{29}$$

$$F_t = \text{rand} \times (M_t \times (-v_t + V_{tp})), \tag{30}$$

Position update:

$$X_i^{new} = X_{best} + (\alpha \times (1 - r_2) + r_2) \times (U_2 \times X_{best} - X_i) - S, \tag{31}$$

where $S = \text{rand} \times U_2 \times Y_t \times F_t$, $v_t = X_i$ and, $V_{tp}$ is a randomly selected individual position.

The two mechanisms enhance the local search ability by leveraging information such as individual fitness and the global optimal solution. When a solution goes beyond the boundaries, it is randomly re-initialized within the search space:

$$X_{i,j}^{new} = lb_j + \text{rand} \times (ub_j - lb_j), \text{ if } X_{i,j}^{new} \notin [lb_j, ub_j] \tag{32}$$

The algorithm keeps track of the historical optimal position $X_p$ for every individual. When a new solution outperforms the current optimal solution, an update is carried out.

$$X_{p,i} = X_i^{new} \text{ if } f(X_i^{new}) < f(X_{p,i}) \tag{33}$$

2.4.3. CPO-CatBoost Model Computation Process

The CPO-CatBoost model optimizes key parameters of CatBoost through the CPO algorithm to enhance classification performance by minimizing the objective function (e.g., model error), defined as:

$$f(\theta) = 1 - \text{Accuracy}(\theta), \tag{34}$$

where is the vector of parameters to be optimized, and Accuracy is the classification accuracy of CatBoost.

The specific process is as follows:

(1) Determine the CatBoost parameters to be optimized: iterations number, learning rate, tree depth, and random strength.
(2) Initialize the population in the CPO.
(3) For each individual in the population, train a CatBoost model and calculate the classification error.
(4) Update the population via the CPO's exploration and exploitation mechanisms, retaining parameter combinations with lower errors.
(5) After reaching the maximum iteration number, output the optimal parameters.

## 3. Experimental Results and Analysis

### 3.1. Experimental Platform Setup

This section's experimental data acquisition test subject is an S13-M-200/10 transformer. In accordance with the standards and requirements for transformer noise measurement specified in GB/T 1094.10—2003 [38], a condenser microphone was used as the acoustic sensor to measure the transformer core under different degrees of core loosening. The sampling rate was 50 kHz, with a frequency response of 20 Hz–20 kHz to focus on the effective frequency band of transformer vibration.

As shown in Figure 2, the he pretightening force FN was adjusted to 0, 0.20 FN, 0.40 FN, and FN to simulate four distinct levels of core loosening: 100%, 80%, 60%, and 0%. A total of 500 audio files were collected. Subsequently, the dataset was partitioned into training, validation, and test sets at a 6:2:2 ratio as detailed in Table 1, serving the purpose of comprehensive training, validation, and testing.



**Figure 2.** Fault Configuration.

**Table 1.** Experimental Sample Data.

| Tags | Fault Type | Training Set | Validation Set | Test Set |
|---|---|---|---|---|
| 1 | 60% Looseness | 80 | 27 | 27 |
| 2 | 80% Looseness | 80 | 27 | 27 |
| 3 | 100% Looseness | 88 | 29 | 29 |
| 4 | Normal State | 52 | 17 | 17 |

### *3.2. Experimental Diagnosis of Transformer Core Loosening Based on Fusion Feature Extraction and CPO-Optimized CatBoost*

Taking the signal tested with the transformer core loosened by 60% as an example, the IMF decomposition has six layers. Simultaneously, VMD decomposition is performed on the original signal, and spectral analysis is conducted on each IMF layer, as shown in Figure 3.

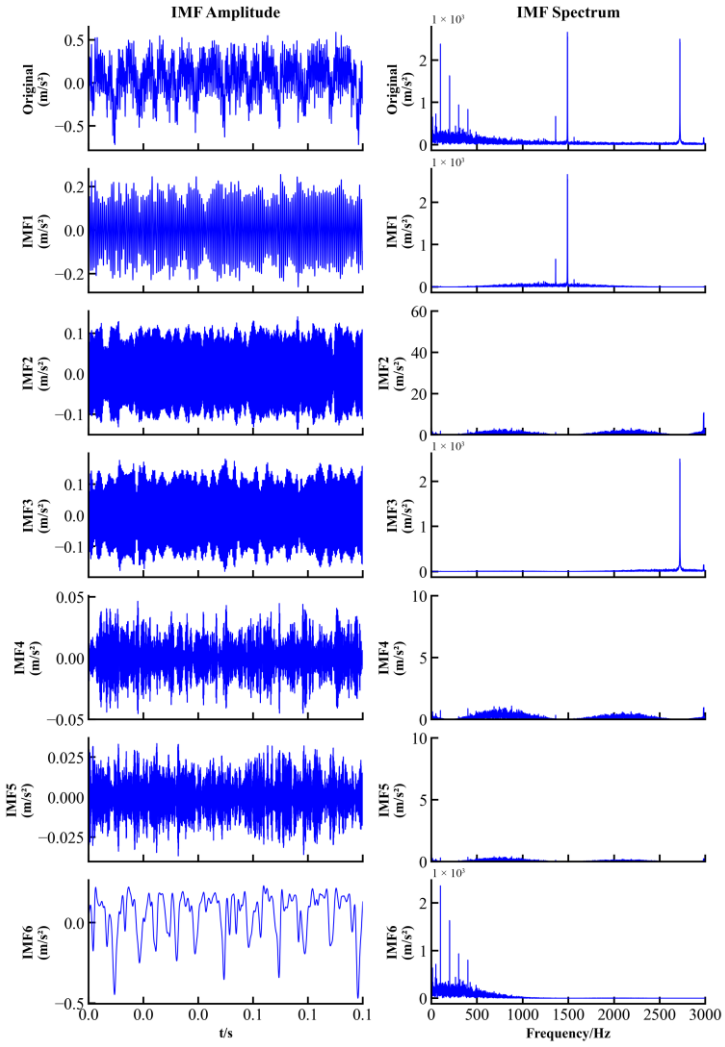



**Figure 3.** Signal VMD Decomposition Diagram and Spectrum Diagram.

Table 2 presents the data results of three indicators, namely the energy proportion, central frequency, and kurtosis of the IMF, as well as the fuzzy entropy, which are obtained through calculations.

As shown in Table 2, the fuzzy entropy values of IMF1, IMF2, IMF3, and IMF6 are all below the threshold of 3.0385, according to Formula (16), indicating they are valid signals. Among these, IMF1 and IMF6 constitute the primary energy components with energy proportions of 31.84% and 40.91%, respectively, while IMF2 and IMF3, with energy proportions of 10.65% and 15.92%, also contain valid information. The central frequencies of IMF1–3 fall within the medium-to-high frequency range, corresponding to the medium-to-high-frequency components in the original signal that contain either routine equipment vibration or faint early-stage fault characteristics. The kurtosis values of IMF1–3 are all close to 3, exhibiting stable fluctuations and possessing the core characteristic of stable signal validity. IMF6 has a central frequency of 426.5 Hz within the low-frequency range, reflecting

low-frequency components indicative of overall equipment vibration characteristics or pronounced fault features. Although IMF6 exhibits a high kurtosis value, it contains effective signals of fault impacts in transformer core loosening faults, making it a crucial manifestation of fault characteristics.

**Table 2.** Calculation Results of Energy Proportion, Central Frequency, Kurtosis, and Fuzzy Entropy of Each Layer of IMF.

| IMF | Energy Proportion (%) | Central Frequency (Hz) | Kurtosis | Fuzzy Entropy |
|---|---|---|---|---|
| IMF1 | 31.84% | 1522.9 Hz | 2.69 | 0.1488 |
| IMF2 | 10.65% | 4279.7 Hz | 2.48 | 0.3810 |
| IMF3 | 15.92% | 2901.0 Hz | 2.49 | 0.2016 |
| IMF4 | 0.42% | 6619.8 Hz | 4.77 | 3.3226 |
| IMF5 | 0.26% | 9892.1 Hz | 4.55 | 4.0540 |
| IMF6 | 40.91% | 426.5 Hz | 5.63 | 0.3820 |

Meanwhile, IMF4 and IMF5 exhibit fuzzy entropy values of 3.3226 and 4.0540, exceeding the threshold, yet their energy proportions are only 0.42% and 0.26%, respectively—far lower than those of the other four IMFs. Combined with central frequency analysis, IMF4 and IMF5 exhibit high frequencies of 6619.8 Hz and 9892.1 Hz, respectively, with kurtosis values of 4.77 and 4.55. This indicates that components 4 and 5 contain substantial noise components requiring removal. Feature extraction is then performed on the denoised signal, which is input into the CPO-CatBoost model for parameter optimization and fault classification diagnosis.

To comprehensively evaluate the practical effectiveness of the proposed CPO-CatBoost algorithm in diagnosing transformer core loosening faults, this section designs a systematic comparative experimental plan. The experiment partitions the dataset into training, test, and validation sets with a ratio of 6:2:2.

The experiments compare the fault recognition performance of four MFCC variants under CatBoost and CPO-CatBoost: 24-dimensional fused MFCC features with VMD denoising, 39-dimensional traditional MFCC with VMD denoising, 24-dimensional fused MFCC without VMD denoising, and 39-dimensional traditional MFCC without VMD denoising. For brevity, the following abbreviations are used throughout: VMD-24D MFCC, VMD-39D MFCC, 24D MFCC, and 39D MFCC. The experimental environment configuration is as follows: population size of 30, maximum iteration number of 50. Within CatBoost's parameters, the iteration number is set to [50~300], learning rate is set to [0.001, 1], tree depth to [4~8], and random strength to [1~6].

As shown in Figure 4, for the VMD-24D MFCC, the fault recognition accuracy under the standard CatBoost classifier is 93.1273%. After the optimization of CatBoost by CPO, the fault recognition accuracy of VMD-24D MFCC reaches 99.0196%. The parameters derived from the optimization of the standard CatBoost classifier by CPO are listed in Table 3. The error curve drops from 0.019608 at the onset to 0.009804. This clearly demonstrates the effectiveness of the CPO-based optimization strategy in enhancing the performance of the CatBoost classifier for fault recognition tasks.

**Table 3.** Optimal Parameters.

| Parameter | Iteration Count | Learning Rate | Tree Depth | Random Strength |
|---|---|---|---|---|
| Optimal Parameters | 107 | 0.1345 | 3 | 3 |

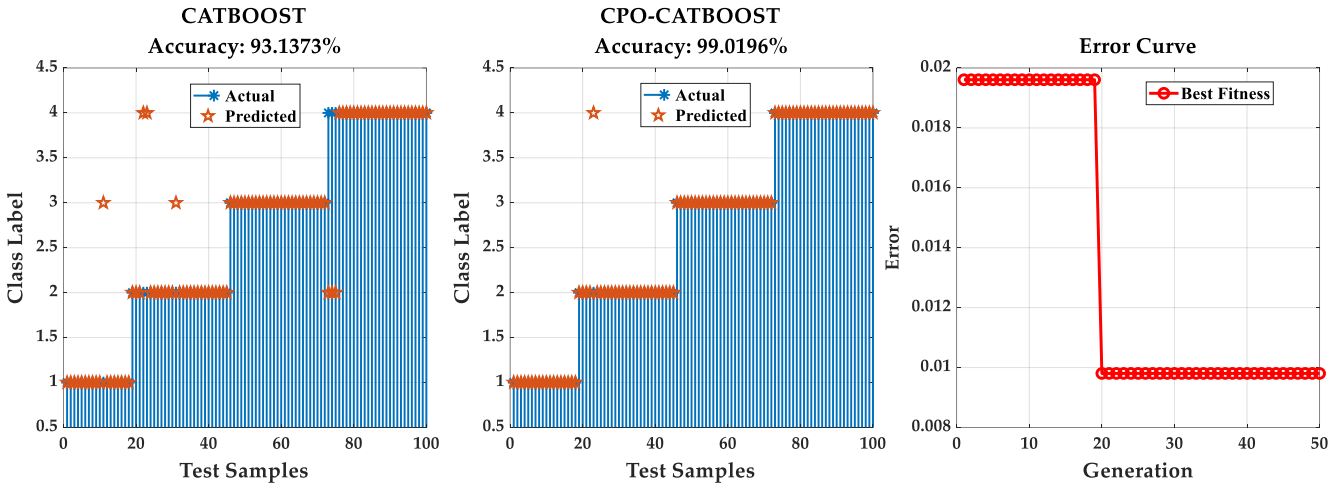



**Figure 4.** Comparison of Standard CatBoost and Optimized CatBoost.

Experiments yielded fault recognition accuracies of 88.5448%, 85.7965%, and 83.9735% for VMD-39D MFCC, 24D MFCC, and 39D MFCC, respectively, under the standard CatBoost algorithm. As shown in Figure 5, this graph illustrates the convergence process over 50 iterations for four different methods under the CPO-CatBoost algorithm. In the VMD-denoised signals, VMD-24D MFCC improved its fault recognition accuracy from 98.0392% to 99.0196% within 19 iterations; VMD-39D MFCC started at only 93.2069% accuracy and reached 95.4823% after 29 iterations. Without denoising, the 24D MFCC fault recognition accuracy increased from 90.5517% to 93.4310% after 27 iterations. The 39D MFCC started at an initial accuracy of 87.4173% and only barely exceeded 90% after 36 iterations, reaching 91.7691%.

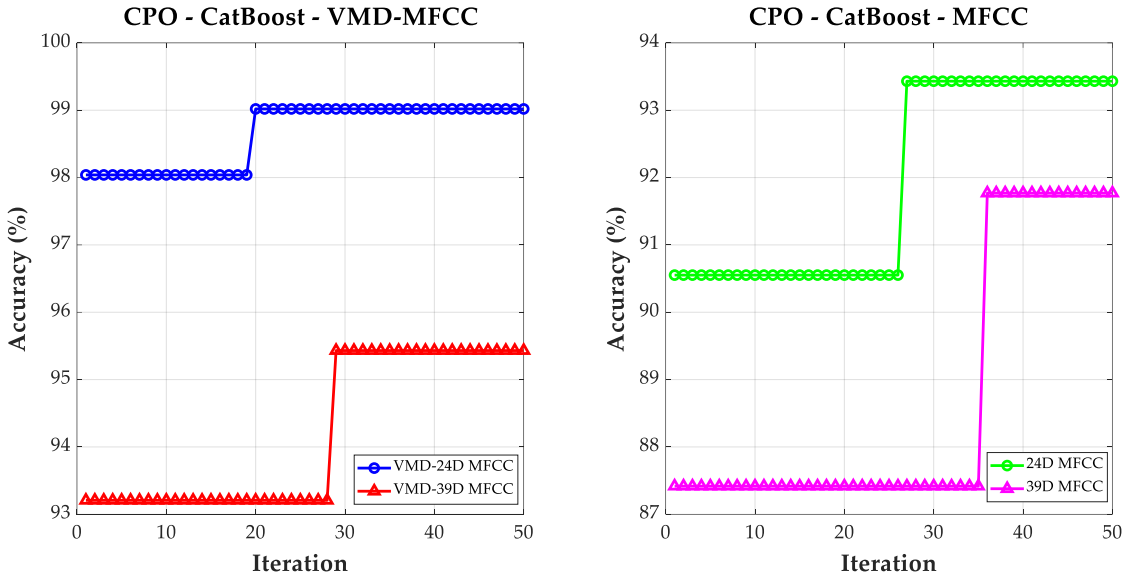



**Figure 5.** Iterative Curves for Different Optimization Algorithms. Iteration Curves for Four CPO-CatBoost Algorithm Configurations.

Figure 6 presents the confusion matrix for fault recognition in the test set, comparing VMD-24D MFCC under standard CatBoost and CPO-optimised CatBoost. It clearly demonstrates that CPO-CatBoost achieves a fault recognition accuracy of 99.0169%, surpassing standard CatBoost by approximately 6%. For normal conditions with transformer core loosening, the recognition rate reached 100%, exceeding the standard by 5.8824%. Under a 60% core loosening fault scenario, the recognition rate was 96.0784%, surpassing

the standard by 7.4074%. Both methods achieved zero errors in the 80% fault scenario. For the 100% core loosening fault condition, the CPO-optimised CatBoost reduced the fault recognition error rate by 10.4573%, achieving 100% accuracy. The VMD-24D MFCC achieved near-perfect classification with the CPO-CatBoost classifier, demonstrating that the CPO-optimised algorithm significantly enhances classification accuracy. CPO optimisation effectively boosts the classification performance of the CatBoost algorithm.

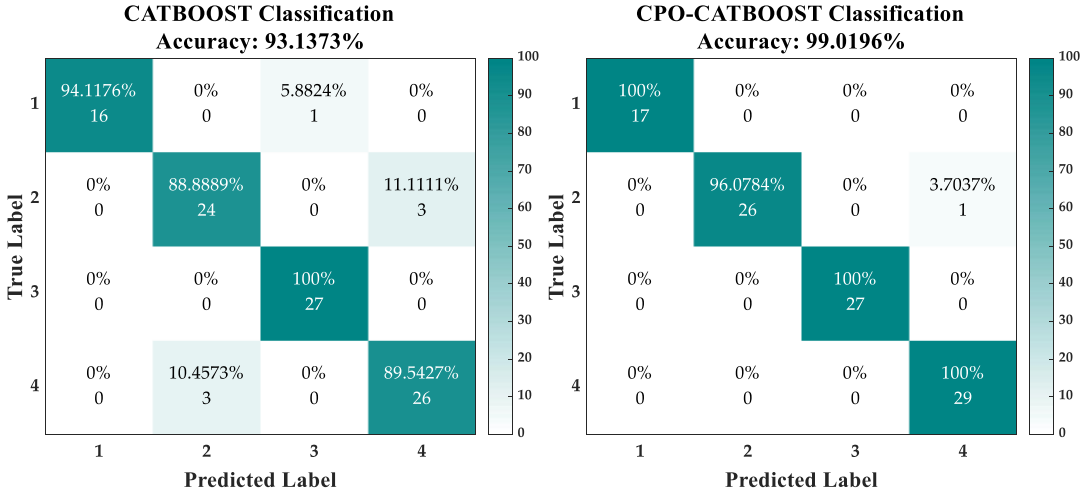



**Figure 6.** Confusion Matrix Comparison of CATBOOST and CATBOOST-CPO Classification Results.

The trained model identifies three distinct fault states and one normal state within the validation set. Table 4 compares the performance of four algorithms in detecting transformer core loosening. Results show that VMD-24D MFCC delivers the best performance, achieving near-perfect accuracy across all conditions—whether 60%, 80%, 100% loosening, or normal state—with an overall accuracy of 99.0196%. Next was VMD-39D MFCC, with an average recognition accuracy of 95.4823%. The 24D MFCC and 39D MFCC algorithms achieved recognition accuracies of only 93.3475% and 91.7691%, respectively. It is evident that incorporating VMD processing significantly improves recognition accuracy, with the 24-dimensional features performing better than the traditional 39-dimensional ones.

**Table 4.** Fault Recognition Accuracy of Four CPO-CatBoost Algorithm Configurations Under Different Loosening States of Transformer Cores.

| Algorithm Configuration | 60% Looseness | 80% Looseness | 100% Looseness | Normal State | Average |
|---|---|---|---|---|---|
| VMD-24D MFCC | 100% | 96.0784% | 100% | 100% | 99.0196% |
| VMD-39D MFCC | 92.8169% | 96.4813% | 100% | 92.6310% | 95.4823% |
| 24D MFCC | 93.6815% | 94.8625% | 97.7448% | 87.4353% | 93.3475% |
| 39D MFCC | 88.4649% | 92.9633% | 96.6890% | 88.9592% | 91.7691% |

To evaluate model performance, the development set was constructed by combining the training and validation sets as per Table 1. Five-fold cross-validation [39] was employed on the development set to assess the performance of CPO-CatBoost under different feature configurations. The evaluation results are presented in Table 5.

To validate the generalisability of the proposed method, 5-fold cross-validation was employed to evaluate the performance of CPO-CatBoost under different feature configurations. Results indicate that the fault recognition accuracy for the VMD-24D MFCC features reached 97.9167% $\pm$ 1.2758%. The test model's fault recognition accuracy was 99.0196%. While marginally higher than the cross-validation mean, it falls within the predicted performance range (96.6409–99.1925%), indicating no degradation or overfitting.

This further validates the model's practical utility. The fault recognition accuracy of VMD-39D MFCC reached 94.1667% ± 1.3975%. The standard deviations for 24D MFCC and 39D MFCC without VMD preprocessing were 2.6160% and 2.9141%, respectively. Comparative analysis revealed that the 24-dimensional features exhibited greater stability than the 39-dimensional features, demonstrating the crucial role of feature preprocessing and dimensionality optimisation in enhancing the model's generalization capability.

**Table 5.** Fault Recognition Accuracy of Four CPO-CatBoost Algorithm Configurations Through Cross-Validation.

| Algorithm Configuration | Fold 1 | Fold 2 | Fold 3 | Fold 4 | Fold 5 | Mean ± SD |
|---|---|---|---|---|---|---|
| VMD-24D MFCC | 97.9167% | 97.9167% | 96.8750% | 100% | 96.8750% | 97.9167% ± 1.2758% |
| VMD-39D MFCC | 92.7083% | 92.7083% | 94.7917% | 95.8333% | 94.7917% | 94.1667% ± 1.3975% |
| 24D MFCC | 86.6432% | 90.7765% | 91.5543% | 93.8876% | 90.8684% | 90.7460% ± 2.6160% |
| 39D MFCC | 85.2345% | 88.7654% | 91.9543% | 87.5432% | 89.1234% | 88.5242% ± 2.9141% |

### *3.3. Model Comparison*

Having established classification accuracy based on the VMD-24D MFCC and CPO-CatBoost models, we further conducted comparative analysis with mainstream algorithmic models in this field: First, the same dataset was processed using VMD-24D MFCC. The processed data were then input into traditional SVM [40], CPO-SVM [41] (a support vector machine based on the CPO optimisation algorithm), and 3D-CNN [42] (a three-dimensional convolutional neural network). The diagnostic results are presented in Figures 7–9.

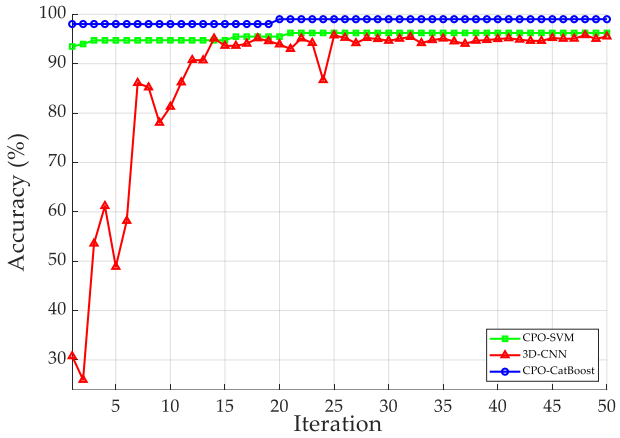



**Figure 7.** Iterative Curves for Different Optimization Algorithms.

Figure 7 illustrates the fault recognition accuracy curves of the three algorithmic models on the training set. The SVM algorithm achieved a fault recognition accuracy of 76%. Observing the training process, the CPO-CatBoost algorithm demonstrated optimal learning capability, with its fault recognition accuracy exceeding 98% in the early iterations and remaining stable thereafter. After 19 iterations, it maintained a high accuracy of 99% with exceptional stability. The CPO-SVM algorithm's fault recognition accuracy rapidly increased from 93% to 94% within the first 15 iterations. Subsequently, it rose from 95% to 96% and remained stable, demonstrating excellent fitting stability. The 3D-CNN algorithm exhibited low initial accuracy (25–30%). After approximately 12 iterations, fault recognition accuracy improved to 92–95%, ultimately stabilising near 95%. However, significant fluctuations occurred during training—for instance, accuracy dropped to 86% at the 24th iteration—reflecting the algorithm's instability during training. Experimental results demonstrate that the CPO-CatBoost algorithm not only exhibits the fastest convergence speed and highest training accuracy but also delivers the most stable training process.

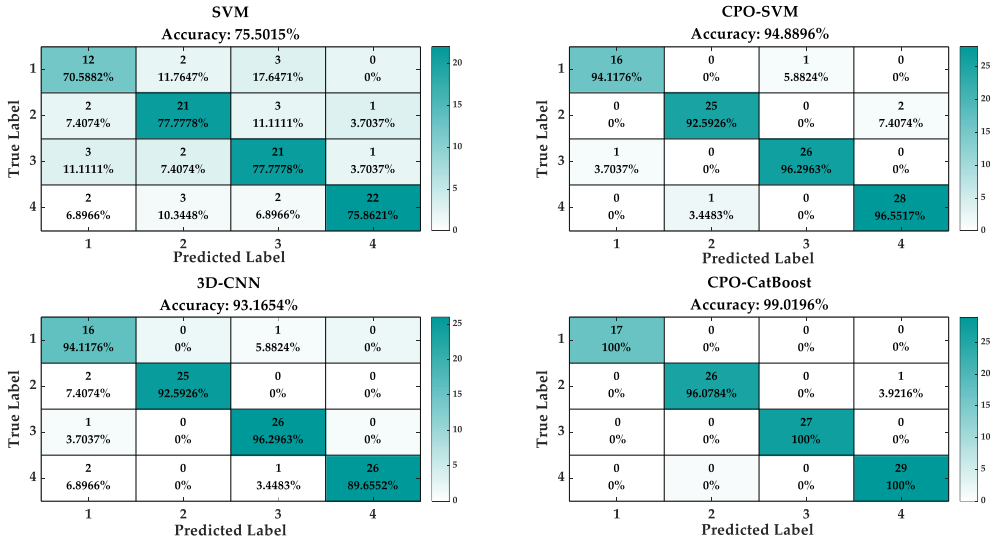



**Figure 8.** Comparison of Confusion Matrices for Classification Results Across Four Models.

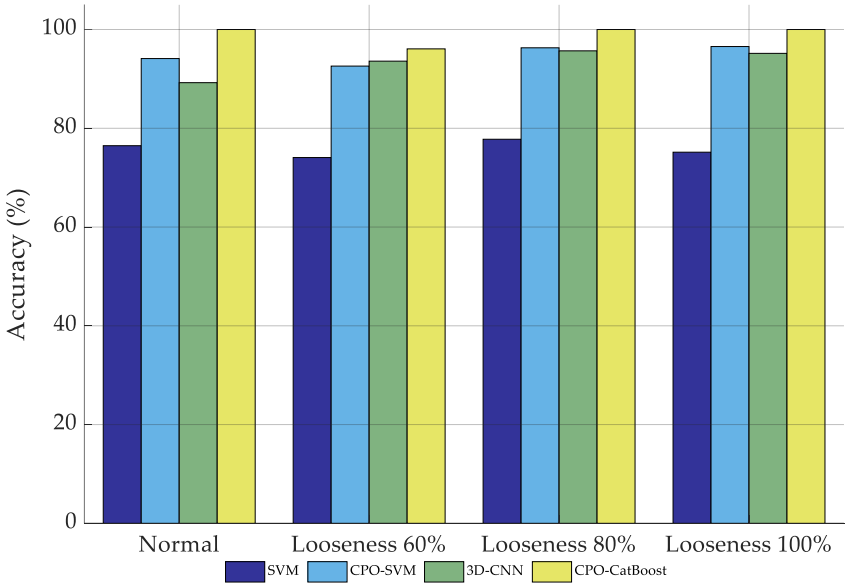



**Figure 9.** Comparison of Diagnostic Results Across Different Models.

Figure 8 shows the performance of four algorithm models on the validation set. The fault recognition accuracy of the traditional SVM model is 75.5015%, with a relatively high rate of misjudgment. In contrast, the fault recognition accuracy of the CPO-SVM model has significantly increased to 94.8896%, with a substantial reduction in misjudgments. The 3D-CNN model achieves a fault recognition accuracy of 93.1654%, with recognition rates for normal core, 60% core looseness, and 80% core looseness all exceeding 90%, specifically 94.1176%, 92.5926%, and 96.2963%, respectively. The CPO-CatBoost model performs the best, with a fault recognition accuracy as high as 99.0196%. Among them, the recognition accuracy for normal core, 80% core looseness, and 100% core looseness all reach 100%, and the recognition accuracy for 60% core looseness is 96.0784%. This fully validates the model's excellent fault recognition capability, indicating its high reliability and practical value in real-world applications, and its ability to provide accurate and reliable classification results for unknown samples.

Figure 9 presents the comparison results of transformer core loosening fault recognition accuracy across four algorithmic models on the test dataset. Among these, the CPO-CatBoost algorithm demonstrated outstanding performance, achieving 100% fault

recognition accuracy across test samples under three operating conditions: normal transformer core state, 80% core loosening, and 100% core loosening. It also maintained a high accuracy rate exceeding 96% under the 60% core loosening condition. The CPO-SVM algorithm demonstrated robust performance, with fault recognition accuracy ranging from 92.5926% to 96.5517% across all four conditions, indicating strong robustness. The 3D-CNN algorithm's fault recognition accuracy ranged from 89.2353% to 95.6784%, slightly underperforming the other two. By contrast, the unoptimised SVM algorithm performed poorly, achieving fault recognition accuracy of merely 74.0741% to 77.7778%. The test results fully validate that the CPO-CatBoost algorithm, optimised through the CPO process, possesses superior fault recognition capabilities, providing reliable technical support for core loosening fault diagnosis.

To validate the generalization capability of the proposed method, the development set was constructed by combining the training and validation sets as per Table 1. Five-fold cross-validation was employed on the development set to evaluate the performance of four models: CPO-CatBoost, CPO-SVM, 3D-CNN, and traditional SVM. The evaluation results are presented in Table 6.

**Table 6.** Fault Recognition Accuracy of Four Different Algorithms in Cross-Validation.

| Algorithm | Fold 1 | Fold 2 | Fold 3 | Fold 4 | Fold 5 | Mean ± SD |
|---|---|---|---|---|---|---|
| CPO-CatBoost | 97.9167% | 97.9167% | 96.8750% | 100% | 96.8750% | 97.9167% ± 1.2758% |
| CPO-SVM | 96.0000% | 93.9394% | 94.0000% | 94.0000% | 91.0000% | 93.7879% ± 1.7874% |
| 3D-CNN | 92.5127% | 89.8543% | 91.4632% | 88.4765% | 94.0123% | 91.2638% ± 2.174% |
| SVM | 73.0000% | 66.0000% | 74.0000% | 78.0000% | 70.7071% | 72.3414% ± 4.4184% |

The stability of other mainstream algorithms was compared and analyzed through 5-fold cross-validation. The fault recognition accuracy rates of CPO-SVM and 3D-CNN were 93.7879% ± 1.7874% and 91.2638% ± 2.174%, respectively. The fault recognition accuracy rate of traditional SVM was the lowest at 72.3414% ± 4.4184%. The fault recognition accuracy rate of CPO-CatBoost was 97.9167% ± 1.2758%. Notably, although the test set accuracy was slightly higher than the cross-validation average, the model did not show a significant performance decline on completely independent data, eliminating the risk of overfitting. Cross-validation provided a relatively conservative performance estimate. The algorithm model in this paper was significantly superior to other methods, maintaining high performance stably on each fold of data and demonstrating excellent generalization ability.

Following all the aforementioned comparisons, the VMD-24D MFCC-CPO-CatBoost approach achieves a significant enhancement in the accuracy of transformer core loosening fault identification through the synergistic effects of VMD preprocessing, MFCC optimal dimension selection, and CPO optimisation. This provides an efficient and reliable solution for the intelligent identification of transformer core loosening faults, demonstrating considerable practical value.

### *3.4. Noise Robustness Testing*

Transformers face complex electromagnetic interference, mechanical vibration, and environmental noise in actual operating environments. These interference factors severely impact signal quality, posing significant challenges to the robustness of fault diagnosis systems. To evaluate the proposed algorithm's robustness in noisy environments, a systematic noise testing protocol was designed. By superimposing Gaussian white noise of varying intensities onto the original audio signal, noise conditions with signal-to-noise ratios (SNR) of 30 dB, 25 dB, 20 dB, 15 dB, 10 dB, 5 dB, and 0 dB were simulated. The 0 dB condition represents an extreme adverse scenario where noise power equals signal power.

In Figure 10, without VMD denoising preprocessing, system performance is severely constrained, and traditional MFCC without VMD denoising is significantly impacted by noise. Under standard CatBoost and CPO optimization, 24D MFCC starts with extremely low fault recognition accuracy of 17.0833–22.5417% at 0 dB, gradually climbing to 85.6250–91.8750% at 30 dB. CPO optimization delivers approximately a 10% improvement in the medium-to-high SNR range. The 39D MFCC performed worst, achieving only 15.6583–19.1667% fault recognition accuracy at 0 dB and 70.2083–75.3750% at 30 dB. This indicates that without effective denoising preprocessing, noise severely interferes with MFCC's feature extraction, drastically reducing feature discriminative power. Even the advanced CatBoost classifier, optimized by the CPO algorithm, struggles to accurately identify fault modes from noise-corrupted features.

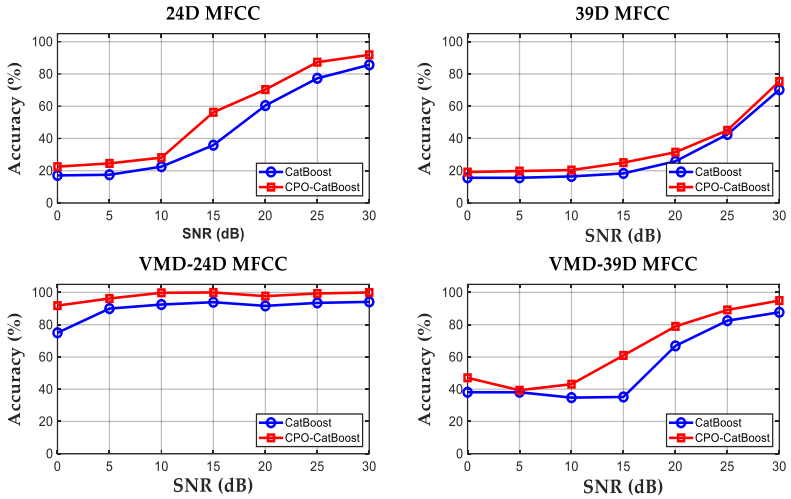



**Figure 10.** Fault Recognition Accuracy in Different Noise Environments.

When employing VMD noise reduction preprocessing, the system demonstrates outstanding noise robustness and fault identification capabilities. Experimental results show that VMD preprocessing significantly enhances the system's noise resistance. The VMD-24D MFCC model delivered the best performance, maintaining a high fault recognition accuracy ranging from 91.8333–99.0196% throughout the entire process after CPO optimization. Its performance curve remained nearly flat at 100%. In contrast, the standard model's fault recognition accuracy gradually increased from 75.1517% to 94.1667%. For VMD-39D MFCC, both models achieved only around 40% fault recognition accuracy at low SNR (0–10 dB) but rapidly improved beyond 15 dB, reaching 87.7083% and 94.95836% at 30 dB, respectively. After applying VMD denoising, the 24-dimensional CatBoost scheme optimized with CPO still achieves over 90% fault recognition accuracy in a 0 dB high-noise environment. These comparative results conclusively demonstrate that VMD denoising technology effectively extracts key modal information from signals, filters out noise interference, and enhances signal quality.

## 4. Discussions and Conclusions

This paper proposes a transformer core loosening fault diagnosis method based on a CatBoost model optimized with CPO and featuring integrated feature extraction. The VMD algorithm decomposes the signal, while fuzzy entropy is applied for noise reduction. Following denoising, the wavelet packet transform is used to optimize feature extraction from standard MFCCs. Concurrently, CPO is incorporated into the parameter optimization selection of the CatBoost model.

In diagnosing transformer core loosening faults, CPO optimizes key parameters of the CatBoost classifier (iteration number, learning rate, tree depth, and random strength). Experimental results demonstrate that the optimized CatBoost achieves significantly improved performance with higher recognition accuracy compared to the standard model. Replacing the short-time Fourier transform with the wavelet packet transform to optimize MFCC yields a 24-dimensional fusion feature (WPT-MFCC). The first eight dimensions represent band energy features; dimensions 9–14 denote intelligent differential features; dimensions 15–19 correspond to core statistical features; and dimensions 20–24 constitute composite statistical features. Comparative experiments demonstrated that the 24-dimensional WPT-MFCC fusion features achieved superior fault recognition accuracy compared to traditional 39-dimensional MFCC features. Considering the extremely complex noise environment surrounding transformers, comprehensive testing was conducted across seven different signal-to-noise ratio levels (0–30 dB). Results demonstrate that introducing VMD for signal decomposition, processing three parameters—energy proportion, central frequency, and kurtosis—using Gaussian membership functions, calculating fuzzy entropy, and employing adaptive thresholding to better distinguish noise and signal components effectively mitigates complex environmental noise impacts. This approach enables the system to exhibit outstanding noise resistance.

Given that mechanical faults such as transformer core loosening adversely impact grid security, this paper proposes a core loosening fault diagnosis model integrating feature extraction with a CatBoost algorithm optimised by the CPO method. Its specific advantages are considerable: In feature processing, WPT replaces the conventional short-time Fourier transform to optimise MFCC. The resulting 24-dimensional MFCC features demonstrate superior fault recognition accuracy compared to traditional 39-dimensional MFCC features. During signal preprocessing, VMD is employed for noise reduction, effectively filtering out interference and improving signal quality, thereby mitigating the adverse impact of noise on fault recognition accuracy. Regarding overall model performance, comparative experimental results demonstrate that the proposed VMD-24D MFCC-CPO-CatBoost model not only achieves higher fault recognition accuracy than other mainstream fault diagnosis algorithms but also consistently maintains stable high-performance behaviour.

However, the experiment is currently limited to its applicability to the present research subjects. Further optimization and analysis are required for different environments and various transformer models to address the following shortcomings:

(1) Samples were collected in a laboratory setting, lacking validation data from complex operational environments. Additionally, testing was conducted only on four distinct levels of core loosening in transformers. The dataset should be expanded to include greater diversity, and the single fault type should be supplemented to account for scenarios involving multiple concurrent faults.
(2) The current VMD mode number is set to a fixed value. In the future, this parameter may be dynamically adjusted based on the inherent complexity of the signal itself. This will enable more effective filtering of various noise components introduced by complex environments within the signal, thereby adapting to noise reduction processing for signals from different types of transformers. This allows the proposed method to transcend the limitations of laboratory environments and better align with practical application scenarios.
(3) At the industrial application level, technical solutions require further alignment with practical requirements. Given the pronounced shortcomings in rapid processing capabilities of traditional, outdated industrial embedded devices and industrial control systems, subsequent efforts must prioritise optimising the compatibility of these

technologies with such equipment and systems. This will ensure their effective implementation and fulfilment of the operational demands of industrial production.

This research provides an effective technical solution for diagnosing transformer core loosening faults. It holds significant reference value for improving power equipment operation and maintenance while ensuring the safe and stable operation of power grids.

**Author Contributions:** Methodology, Y.X.; writing—original draft preparation, Y.X.; writing—review and editing, Y.Z.; investigation, J.X.; data curation, Y.Y.; project administration, Y.Z. All authors have read and agreed to the published version of the manuscript.

**Funding:** This research was funded by the 2025 Jilin Provincial Department of Education Natural Science Research Project (JJKH20250811KJ).

**Data Availability Statement:** The data used to support the findings of this study are available from the corresponding author upon request.

**Conflicts of Interest:** The authors declare that there are no conflicts of interest regarding the publication of this paper.

## References

1. Secic, A.; Krpan, M.; Kuzle, I. Vibro-Acoustic Methods in the Condition Assessment of Power Transformers: A Survey. *IEEE Access* **2019**, *7*, 83915–83931. [CrossRef]
2. Borucki, S. Diagnosis of Technical Condition of Power Transformers Based on the Analysis of Vibroacoustic Signals Measured in Transient Operating Conditions. *IEEE Trans. Power Deliv.* **2012**, *27*, 670–676. [CrossRef]
3. Freire, N.M.A.; Cardoso, A.J.M. Fault detection and condition monitoring of PMSGs in offshore wind turbines. *Machines* **2021**, *9*, 260. [CrossRef]
4. Bagheri, M.; Zollanvari, A.; Nezhivenko, S. Transformer Fault Condition Prognosis Using Vibration Signals Over Cloud Environment. *IEEE Access* **2018**, *6*, 9862–9874. [CrossRef]
5. An, Q.; Li, P.; An, G.; Liu, D. Improved crested porcupine optimizer-VMD method applied to partial discharge signal. *Measurement* **2025**, *258*, 119145. [CrossRef]
6. Liu, H.; Xu, Q.; Han, X.; Wang, B.; Yi, X. Attention on the key modes: Machinery fault diagnosis transformers through variational mode decomposition. *Knowl.-Based Syst.* **2024**, *289*, 111479. [CrossRef]
7. Jian, X.; Hong, M. Transformer winding looseness fault diagnosis based on VMD and WOA—SVM. *Electr. Mach. Control. Appl.* **2023**, *50*, 84–90.
8. Jiao, S.; Shi, W.; Yang, Y. Denoising of UHF partial discharge signals by using VMD based on Shannon entropy and kurtosis-approximation entropy. In Proceedings of the 2019 14th IEEE Conference on Industrial Electronics and Applications (ICIEA), Xi'an, China, 19–21 June 2019; pp. 1742–1747.
9. Wibawa, I.; Darmawan, I. Implementation of audio recognition using mel frequency cepstrum coefficient and dynamic time warping in wirama praharsini. *J. Phys. Conf. Ser.* **2021**, *1722*, 012014. [CrossRef]
10. Rezaul, K.M.; Jewel; Islam, S.; Alam Siddiquee, K.N.e.; Barua, N.; Rahman, M.A.; Shan-A-Khuda, M.; Bin Sulaiman, R.; Shaikh, S.I.; Hamim, A.; et al. Enhancing Audio Classification Through MFCC Feature Extraction and Data Augmentation with CNN and RNN Models. *Int. J. Adv. Comput. Sci. Appl.* **2024**, *15*, 37–53. [CrossRef]
11. Nandan, D.; Singh, M.K.; Kumar, S.; Yadav, H.K. Speaker identification based on physical variation of speech signal. *Trait. Du Signal* **2022**, *39*, 711. [CrossRef]
12. Bhardwaj, V.; Ben Othman, M.T.; Kukreja, V.; Belkhier, Y.; Bajaj, M.; Goud, B.S.; Rehman, A.U.; Shafiq, M.; Hamam, H. Automatic speech recognition (asr) systems for children: A systematic literature review. *Appl. Sci.* **2022**, *12*, 4419. [CrossRef]
13. Azim Naz, M.; Sarath, R. Combined classification models for bearing fault diagnosis with improved ICA and MFCC feature set. *Adv. Eng. Softw.* **2022**, *173*, 103249. [CrossRef]
14. Yan, H.; Bai, H.; Zhan, X.; Wu, Z.; Wen, L.; Jia, X. Combination of VMD mapping MFCC and LSTM: A new acoustic fault diagnosis method of diesel engine. *Sensors* **2022**, *22*, 8325. [CrossRef] [PubMed]
15. Hu, Y.; Zheng, J.; Huang, H. Experimental research on power transformer vibration distribution under different winding defect conditions. *Electronics* **2019**, *8*, 842. [CrossRef]
16. Li, H.; Yao, Q.; Li, X. Voiceprint fault diagnosis of converter transformer under load influence based on Multi-Strategy improved Mel-Frequency spectrum coefficient and Temporal convolutional network. *Sensors* **2024**, *24*, 757. [CrossRef] [PubMed]

17. Xu, J.; Xiao, Y.; Yin, Y.; Zhang, Y. Research on the Fault Diagnosis Method of Rolling Bearings Based on GAVOA–VMD. *J. Electr. Comput. Eng.* **2025**, *2025*, 5650232. [CrossRef]
18. Wang, F.; Wang, S.; Chen, S.; Yuan, G.; Zhang, J. Voiceprint recognition model of power transformers based on improved MFCC and VQ. *Proc. CSEE* **2017**, *37*, 289–297.
19. Cohen, M.X. A better way to define and describe Morlet wavelets for time-frequency analysis. *NeuroImage* **2019**, *199*, 81–86. [CrossRef]
20. Wang, Y.; Xu, G.; Liang, L.; Jiang, K. Detection of weak transient signals based on wavelet packet transform and manifold learning for rolling element bearing fault diagnosis. *Mech. Syst. Signal Process.* **2015**, *54–55*, 259–276. [CrossRef]
21. Mao, M.; Xu, B.; Sun, Y.; Tan, K.; Wang, Y.; Zhou, C.; Zhou, C.; Yang, J. Application of FCEEMD-TSMFDE and adaptive CatBoost in fault diagnosis of complex variable condition bearings. *Sci. Rep.* **2024**, *14*, 30448. [CrossRef]
22. Pan, X.; Zhao, D.; Chen, H.; Shen, A.; Wu, K. Incipient fault identification method for 10 kV power cables based on sheath current and DVAE-SAO-CatBoost. *Electr. Power Syst. Res.* **2025**, *245*, 111583. [CrossRef]
23. Yang, X.S. Nature-inspired optimization algorithms: Challenges and open problems. *J. Comput. Sci.* **2020**, *46*, 101104. [CrossRef]
24. Liu, E.J.; Hung, Y.H.; Hong, C.W. Improved metaheuristic optimization algorithm applied to hydrogen fuel cell and photovoltaic cell parameter extraction. *Energies* **2021**, *14*, 619. [CrossRef]
25. Ye, F. Particle swarm optimization-based automatic parameter selection for deep neural networks and its applications in large-scale and high-dimensional data. *PLoS ONE* **2017**, *12*, e0188746. [CrossRef]
26. Adalja, D.; Patel, P.; Mashru, N.; Jangir, P.; Jangid, R.; Gulothungan, G.; Khishe, M. A new multi objective crested porcupines optimization algorithm for solving optimization problems. *Sci. Rep.* **2025**, *15*, 14380. [CrossRef]
27. Dragomiretskiy, K.; Zosso, D. Variational mode decomposition. *IEEE Trans. Signal Process.* **2013**, *62*, 531–544. [CrossRef]
28. Shang, X.-Q.; Huang, T.-L.; Chen, H.-P.; Ren, W.-X.; Lou, M.-L. Recursive variational mode decomposition enhanced by orthogonalization algorithm for accurate structural modal identification. *Mech. Syst. Signal Process.* **2023**, *197*, 110358. [CrossRef]
29. Sharma, A.; Kaul, S. Two-Stage Supervised Learning-Based Method to Detect Screams and Cries in Urban Environments. *IEEE/ACM Trans. Audio Speech Lang. Process.* **2016**, *24*, 290–299. [CrossRef]
30. Domingo, D.; Kareem, A.B.; Okwuosa, C.N.; Custodio, P.M.; Hur, J.-W. Transformer Core Fault Diagnosis via Current Signal Analysis with Pearson Correlation Feature Selection. *Electronics* **2024**, *13*, 926. [CrossRef]
31. Maliuk, A.S.; Ahmad, Z.; Kim, J.M. A technique for bearing fault diagnosis using novel wavelet packet transform-based signal representation and informative factor LDA. *Machines* **2023**, *11*, 1080. [CrossRef]
32. Chen, Y.; Zhang, T.; Luo, Z.; Sun, K. A novel rolling bearing fault diagnosis and severity analysis method. *Appl. Sci.* **2019**, *9*, 2356. [CrossRef]
33. Jing, Y.; Wang, X.; Yu, Z.; Wang, C.; Liu, Z.; Li, Y. Diagnostic research for the failure of electrical transformer winding based on digital twin technology. *IEEJ Trans. Electr. Electron. Eng.* **2022**, *17*, 1629–1636. [CrossRef]
34. Prokhorenkova, L.; Gusev, G.; Vorobev, A.; Dorogush, A.V.; Gulin, A. CatBoost: Unbiased boosting with categorical features. In Proceedings of the 32nd International Conference on Neural Information Processing Systems, Montréal, QC, Canada, 3–8 December 2018; Volume 31.
35. Yang, M.; Liu, W.; Zhang, W.; Wang, M.; Fang, X. Bearing vibration signal fault diagnosis based on LSTM-cascade CatBoost. *J. Internet Technol.* **2022**, *23*, 1155–1161. [CrossRef]
36. Abdel-Basset, M.; Mohamed, R.; Abouhawwash, M. Crested Porcupine Optimizer: A new nature-inspired metaheuristic. *Knowl.-Based Syst.* **2024**, *284*, 111257. [CrossRef]
37. Liu, H.; Zhou, R.; Zhong, X.; Yao, Y.; Shan, W.; Yuan, J.; Xiao, J.; Ma, Y.; Zhang, K.; Wang, Z. Multi-strategy enhanced crested porcupine optimizer: CAPCPO. *Mathematics* **2024**, *12*, 3080. [CrossRef]
38. *GB/T 1094.10-2003*; Power Transformers—Part 10: Determination of Sound Levels. Standards Press of China: Beijing, China, 2003.
39. Chen, J.; Wang, Y.; Kong, L.; Chen, Y.; Chen, M.; Cai, Q.; Sheng, G. A novel method for power transformer fault diagnosis considering imbalanced data samples. *Front. Energy Res.* **2025**, *12*, 1500548. [CrossRef]
40. Huerta-Rosales, J.R.; Granados-Lieberman, D.; Garcia-Perez, A.; Camarena-Martinez, D.; Amezquita-Sanchez, J.P.; Valtierra-Rodriguez, M. Short-circuited turn fault diagnosis in transformers by using vibration signals, statistical time features, and support vector machines on FPGA. *Sensors* **2021**, *21*, 3598. [CrossRef]
41. He, G.; Feng, L.; Yang, G. A new method for bearing fault diagnosis based on adaptive SVMD and RCMDSE-IDHT. *IEEE Access* **2024**, *12*, 169467–169486. [CrossRef]
42. Cui, J.; Ma, H. Transformer Iron Core Looseness Fault Diagnosis Model Based on CEEMDAN-Wavelet-Threshold and 3D-CNN. *Electr. Mach. Control. Appl.* **2022**, *49*, 46–52.


**Disclaimer/Publisher's Note:** The statements, opinions and data contained in all publications are solely those of the individual author(s) and contributor(s) and not of MDPI and/or the editor(s). MDPI and/or the editor(s) disclaim responsibility for any injury to people or property resulting from any ideas, methods, instructions or products referred to in the content.